American Journal of Mechanical Engineering, 2017, Vol. 5, No. 2, 64-69
Available online at http://pubs.sciepub.com/ajme/5/2/5

DOI:10.12691/ajme-5-2-5

Error Analysis of a Kind of Binocular Visual Alignment Device

Zhi-Ze Wang[1], Zhi-Feng Lou[1,2], Hong-Xia Song[1,2,*], Xiao-Dong Wang[1,2], Xing-Yuan Wang[1]

[1]Key Laboratory for Micro/Nano Technology and System of Liaoning Province, Dalian University of Technology, Dalian, Liaoning, China
[2]Key Laboratory for Precision and Non-traditional Machining of Ministry of Education, Dalian University of Technology, Dalian, Liaoning, China
*Corresponding author: hxsong@dlut.edu.cn

Abstract Precision assemblies of small interference fitting parts are usually achieved by precision press-fit instrument. As the key module of the precision assembly system, the alignment accuracy of the visual alignment device (VAD) directly affects the assembly quality. In this paper, a precision press-fit instrument was introduced, in which contain a kind of binocular visual alignment device. For this kind of VAD is combined with two cameras and a three-dimensional precision displacement platform, a calibration method was introduced in this paper to measure the tilt angle of the guide rail Z, and the error caused by the tilt of the three guide rails of VAD was analyzed. Finally, the final transfer equation between this two cameras was obtained by taking the error into account. The experimental results show that the analytical method can help the press-fit instrument improve the alignment accuracy effectively, and the alignment accuracy can reach ±10μm, so the instrument can meet the requirement of the assembly work.

Keywords: *precision assemblies, visual alignment device, alignment accuracy, transfer equation, tilt angle*

Cite This Article: Zhi-Ze Wang, Zhi-Feng Lou, Hong-Xia Song, Xiao-Dong Wang, and Xing-Yuan Wang, "Error Analysis of a Kind of Binocular Visual Alignment Device." *American Journal of Mechanical Engineering*, vol. 5, no. 2 (2017): 64-69. doi: 10.12691/ajme-5-2-5.

1. Introduction

The device, which is composed of precision micro driver and sensing device, has been widely used in industry, military and biological fields in recent years because of its small size and reliable performance [1]. In order to improve the assembly quality of micro assembly and the consistency of the product, the manual assembly is gradually replaced by the precision automatic assembly instrument. The vision alignment device (VAD) is indispensable in the automatic precision assembly system, which has the advantages of non-contact, flexibility, high precision, high speed, automation and high intelligent level [2]. Using binocular vision to complete the position detection of circular hole and the alignment work can overcome the disadvantages of the traditional positioning method, which needs locating blocks and has poor flexibility [3,4,5], and the alignment accuracy of the VAD directly affects the assembly quality.

The vision alignment device is generally composed of CCD, optical mirror group, light source and three-dimensional precision displacement platform. An extensive research have been done to reduce the visual alignment error. Xin Ye et al [6] proposed a sub-pixel calibration method to reduce the assembly error, caused by the lens' distortion of the VAD. Guihua Liu et al [7] put forward a novel camera calibration method of variable focal length, based on the orthogonal rotation matrix. The intrinsic and extrinsic camera parameters in each image linearly can be calculated by this means as long as at least six known points are captured in each image. The experimental results showed that this method has high accuracy and robust. In order to reduce the error caused by the instability of the light source, Zhaobang Pu et al [8] analyzed the intensity, stability and uniformity of the light source in VAD, and designed ring type cold illumination that can automatic adjust intensity of light. Yonglong Tang et al [9]. studied the alignment error which was caused by the prism mounting error in the vision system of the coaxial optical alignment device, and the influence equation of the error was given. Based on the ruled surface theory, Qijing Tang et al [10] established the mathematical model of ruled surfaces. The overall calibration of the visual detective system was realized, and the visual detection error was controlled within ±3%. Daljae Lee et al [11]. proposed a dual imaging system to achieve high alignment accuracy in chip packaging. A vision servoing algorithm had been designed to determine the direction and speed of translation and rotation, the alignment accuracy and the tracking speed had been improved. Y. S. Ihn et al [12]. introduced a fast vision processing algorithm, a modified binary region median filter combined with a labeling based segmentation scheme, for a machine vision system. This method reduced the processing time, and it helped the system become more stable and less noise sensitive even for the light reflections. CY Nian et al [13] designed three-axis motion control mechanism and applied it into an auto-

alignment vision system. By analyzing the coordinate relationship, the compensation amount in the 3 axis direction is obtained, and the alignment precision was achieved within 5μm.

At present, the method of improving the visual alignment accuracy, which is combined with camera and three-dimensional precision displacement platform, is mostly based on the calibration method, image processing algorithm and visual alignment algorithm. However, the installation error of the guide rail in the device has been not analyzed. For this kind of VAD, even if the two cameras' alignment accuracy is very high, the final alignment accuracy is still largely affected by the mounting precision of the three guide rails. As a result, it is significant to guarantee the alignment precision by making compensation according to the installation error of the camera guide rail. In this paper, the error caused by the installation error between three camera guide rails was analyzed, based on the developed precision press-fit instrument, and the final alignment error transfer equation was deduced.

2. Accuracy Analysis

2.1. Press-fit Instrument and the Small Interference Fitting Parts

As shown in Figure 1, the main frame of the press-fit instrument is composed of four guide shafts and upper and lower beams. In the assembly process, the assembly components are mounted on the upper and lower fixtures which are fixed on the moving beam and XY precision stage respectively. The relative position of the assembly components are measured by the visual alignment device. The adjustment of part's posture is realized by the precision turntable and XY precision stage. The force sensor and linear grating scale are used to measure the pressing force and the displacement of moving beam respectively. The moving beam is driven by a ball screw actuator to move along the guide shaft to complete the press-fit work.

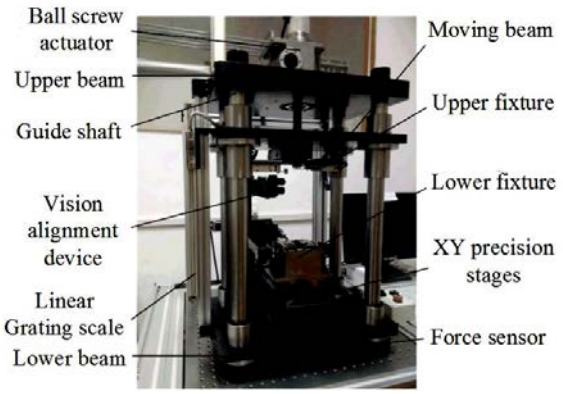

Figure 1. Precision press-fit instrument

As shown in Figure 2, the coaxiality, parallelism and perpendicularity of the small interference fitting parts are required. In this paper, the part which was fixed by the upper fixture was defined as part A, and the part which was fixed by the lower fixture was defined as part B. As shown in Figure 3, the assembly process of the small interference fitting parts was as follows:

1) **Initialization**: Open the press-fit program, initialize the instrument;
2) **Feeding**: Mounting part A and part B on the upper and lower fixture respectively;
3) **Alignment**: Moving the camera along three guide rails to the acquisition position to acquire the two parts' images, then the deviation between two parts can be calculated and the XY precision stage were controlled by the industrial computer to adjust the position of the part B;
4) **Press-fitting**: The ball screw actuator drives moving beam to move down until the press force, fed back by the force sensor, reaches the threshold value n, and then control the moving beam moves up to the origin position;
5) **End**: Take out the assembly part, and prepare the next press work.

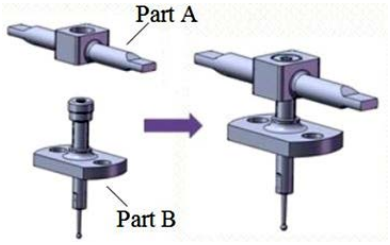

Figure 2. Assembly process of small interference fitting parts

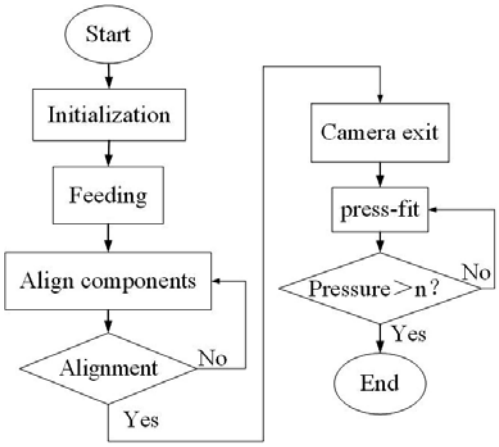

Figure 3. Flowchart for the assembly process of the precision press-fit instrument

2.2. Visual Alignment Device and Alignment Strategy

The VAD (Figure 4) is mainly composed of the following components: two CCD, two light sources, two telecentric lenses, two mirrors and three precision guide rails. The cameras were moved to the image acquisition position by three-dimensional precision displacement platform (composed of X, Y, Z precision guide rail). In the process of coaxial alignment, the upper camera was moved to the image acquisition position to acquire the image of part A, and the image features were transferred into lower camera through the transfer equation. Then, the lower camera was moved to the acquisition position to acquire the image of part B. During the real-time image

processing, the position deviation between part A and part B was calculated by the computer. Meanwhile, the XY precision stage was controlled by the computer to finish the alignment work.

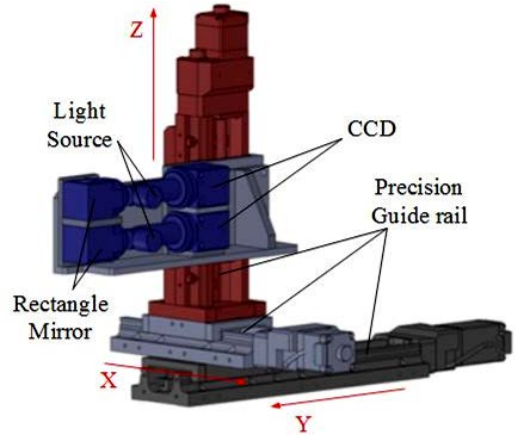

Figure 4. Vision alignment device

The relative position and the coordinate systems of two cameras were shown in Figure 5. The transfer equation between two cameras in this VAD is listed as Equation (1):

$$\begin{bmatrix} S_{u_2} & 0 & 0 \\ 0 & S_{v_2} & 0 \\ 0 & 0 & 1 \end{bmatrix} \begin{bmatrix} u_2 \\ 1200 - v_2 \\ 1 \end{bmatrix} = \begin{bmatrix} \cos\gamma & \sin\gamma & 0 \\ -\sin\gamma & \cos\gamma & 0 \\ 0 & 0 & 1 \end{bmatrix} \begin{bmatrix} S_{u_1} & 0 & 0 \\ 0 & S_{v_1} & 0 \\ 0 & 0 & 1 \end{bmatrix} \begin{bmatrix} u_1 + a \\ v_1 + b \\ 1 \end{bmatrix}. \quad (1)$$

In the above equation, S_{ui}, S_{vi} (i=1, 2) are the physical size per pixel of the camera; a, b are the coordinates of the upper camera's coordinate origin in the lower camera; γ is the angle between the two camera coordinate axes; u_i, v_i are the coordinate value of a point in the upper and lower camera system, respectively.

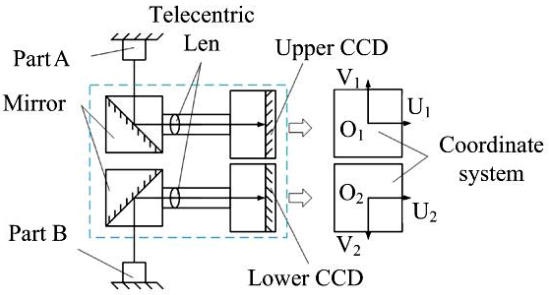

Figure 5. The structure diagram of the upper and lower cameras

2.3. Error Analysis of the Visual Alignment Device

2.3.1. Error Analysis of the Tilt of the Guide Rail Z

The instrument is used to finish the precision assembly work of several kinds of parts. In the assembly and calibration process, due to the height of each part is different, but the camera's focal length is fixed, so the camera's acquisition position of different part should be different. In the calibrating process of the transfer equation, it is too complex and time-consuming to calibrate all acquisition positions. Therefore, to simplify the calibration process, the calibration result of an arbitrary acquisition position is often used in the assembly process of all kinds of parts. So the image acquisition positions in assembling and calibrating processes are different.

As shown in Figure 6, positions 1, 4 are the acquisition positions in the calibrating process. Positions 2, 3 are the acquisition positions in assembly process. If the guide rail Z is tilt relative to the press-fitting direction, the coefficient of transfer equation calculated by the calibration result will be different when the camera is at different heights. Therefore, the tilt of the guide rail Z relative to the press-fitting direction will cause the alignment error.

The coordinate systems of the upper and lower cameras are $U_1O_1V_1$ and $U_2O_2V_2$, respectively (Figure 5). The press-fitting direction is defined as W axis, and the instrument coordinate system is UVW (Figure 6). There is parallelism error between the guide rail Z and the W axis. The angle between guide rail Z and W axis in the UOW and VOW plane were assumed θ_1 and θ_2 respectively. When the upper and lower cameras' displacements along the guide rail Z were ΔL_{Zi} (i = 1,2), the errors caused by the tilt of guide rail Z along the U and V directions in the coordinate system of camera can be calculated by Equation (2).

$$\begin{cases} \Delta U_{iz} = \dfrac{\Delta L_{Zi} \tan\theta_1}{\sqrt{1 + (\tan\theta_1)^2 + (\tan\theta_2)^2}} \\ \Delta V_{iz} = \dfrac{\Delta L_{Zi} \tan\theta_2}{\sqrt{1 + (\tan\theta_1)^2 + (\tan\theta_2)^2}} \end{cases} \quad (2)$$

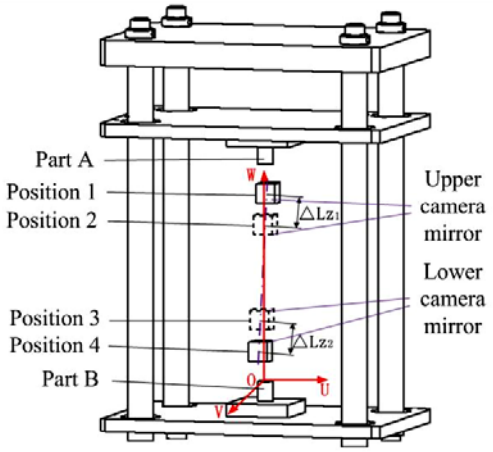

Figure 6. The error analysis diagram of guide rail Z

Since an angle γ exists between axis U_1 and U_2, the angle θ_1 and θ_2 are different. These two angles caused by the tilt of guide rail Z in coordinate system U_1V_1W are defined as θ_{u1} and θ_{u2}. The two angles in coordinate system U_2V_2W are defined as θ_{l1} and θ_{l2}. As shown in Figure 5, the distance along the guide rail Z between position 1 and position 2 is ΔL_{Z1}, and the distance between position 3 and position 4 is ΔL_{Z2}. So the alignment error of two cameras caused by the tilt of guide rail Z can be calculated by Equation (2).

In the alignment process, the features of the image obtained by upper camera will be converted into the lower camera using the transfer equation. So the error in the upper camera will change after converting, and the error caused by ΔL_{z1} in lower camera (Equation (5)) can be deduced out according to the Equation (1).

$$\begin{bmatrix} \Delta U_{1Z}^{'} \\ \Delta V_{1Z}^{'} \end{bmatrix} = \begin{bmatrix} -\cos\gamma & \sin\gamma \\ \sin\gamma & \cos\gamma \end{bmatrix} \begin{bmatrix} \Delta U_{1Z} \\ \Delta V_{1Z} \end{bmatrix}. \tag{3}$$

So the alignment error along U, V direction caused by the tilt of guide rail Z can be expressed as Equation (4):

$$\begin{bmatrix} \Delta U_Z \\ \Delta V_Z \end{bmatrix} = \begin{bmatrix} \Delta U_{1Z}^{'} \\ \Delta V_{1Z}^{'} \end{bmatrix} + \begin{bmatrix} \Delta U_{2Z} \\ \Delta V_{2Z} \end{bmatrix}. \tag{4}$$

2.3.2. Error Analysis of the Tilt of Guide Rail X and Y

If the deviation of two parts is larger than the camera's view in plane UOV, at this time after capturing image by the upper camera, the lower camera need to be moved along guide rail X, Y, Z to capture the image of part B. So we need to consider the tilt of the guide rail X and Y.

The camera's depth of field is 270μm, experiments showed that the part is not beyond the camera's depth of field when the camera moves along the guide rail X and Y. so the error caused by the tilt of guide rail X and Y along W direction could be neglected. In the coordinate system U_2V_2W, the projection of the included angle between the camera's guide rail X and axis U_2 in $U_2O_2V_2$ and U_2O_2W are ξ_1 and ξ_2, respectively. The projection of the included angle between the camera's guide rail Y and axis V_2 in $U_2O_2V_2$ and V_2O_2W are ζ_1 and ζ_2 , respectively. The movement distance of camera along the guide rail X and Y are L_x and L_Y respectively. So the alignment error along U and V direction in lower camera caused by L_x and L_Y is listed respectively as follows:

$$\begin{cases} \Delta U_{2x} = (1-\cos\xi)\cdot L_X \\ \Delta V_{2x} = L_X \cdot \sin\xi \end{cases} \tag{5}$$

$$\begin{cases} \Delta U_{2y} = (1-\cos\zeta)\cdot L_Y \\ \Delta V_{2y} = L_Y \cdot \sin\zeta \end{cases} \tag{6}$$

The alignment error caused by the tilt of guide rail X, Y and Z can be expressed as Equation (7):

$$\begin{bmatrix} \Delta u \\ \Delta v \end{bmatrix} = \begin{bmatrix} \Delta U_z \\ \Delta V_z \end{bmatrix} + \begin{bmatrix} \Delta U_{2X} \\ \Delta V_{2X} \end{bmatrix} + \begin{bmatrix} \Delta U_{2Y} \\ \Delta V_{2Y} \end{bmatrix}. \tag{7}$$

Combine with transfer equation of the upper and lower cameras, the final transfer equation can be derived as Equation (8):

$$\begin{bmatrix} S_{u_2} & 0 & 0 \\ 0 & S_{v_2} & 0 \\ 0 & 0 & 1 \end{bmatrix} \begin{bmatrix} u_2 \\ 1200 - v_2 \\ 1 \end{bmatrix} = \begin{bmatrix} \cos\gamma & \sin\gamma & 0 \\ -\sin\gamma & \cos\gamma & 0 \\ 0 & 0 & 1 \end{bmatrix} \begin{bmatrix} S_{u_1} & 0 & 0 \\ 0 & S_{v_1} & 0 \\ 0 & 0 & 1 \end{bmatrix} \begin{bmatrix} u_1 + a \\ v_1 + b \\ 1 \end{bmatrix} + \begin{bmatrix} \Delta u \\ \Delta v \\ 0 \end{bmatrix}. \tag{8}$$

3. Experiment

3.1. Calibrate the Pixel of Two Cameras and the Coefficient of Transfer Equation

As shown in Table 1, the physical size of per pixel was obtained by the calibration of cameras using the optical standard ruler [14].

Table 1. The Results of Pixel Calibration

Camera	S_u (μm/p)	S_v (μm/p)
Upper	4.74	4.74
Lower	4.77	4.77

As shown in Figure 7, the method of measuring the included angle γ is described as follows:

1) Fixing the optical standard ruler on the precision turntable;
2) Moving the upper camera to the acquisition position, turning the turntable to make the transverse line parallel with the U_1 axis;
3) Setting two points A, B on the standard ruler along the direction of transverse line, the distance between this two points is L. The upper camera was controlled to acquire the image of A. Then, the camera was moved L along the transverse line of the standard ruler to acquire the image of B;
4) Processing images to get the coordinates of A (u_{11},v_{11}) and B (u_{12},v_{12});
5) The angle γ_1 between the guide rail X and U_1 axis can be calculated by Equation (9), and the same method can be used to get the angle γ_2 between the guide rail X and U_2 axis. Then $\gamma = \gamma_1 - \gamma_2$.

$$\gamma_1 = \tan^{-1}\frac{S_v\cdot(v_{12}-v_{11})}{L} \tag{9}$$

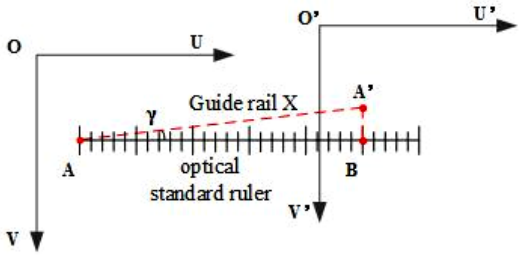

Figure 7. The diagram of measuring the inclination of the guide rail X

The images in upper camera were shown in Figure 8, the results were γ_1=−0.46°, γ_2=0.36° and γ=−0.10°.

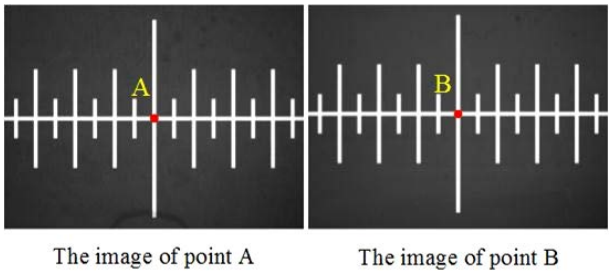

Figure 8. The images of measuring the included angle between guide rail X and axis U_1

The coefficients in the Equation (1) can be calculated by the imprint method which is introduced in the reference [15]. The measurement steps are as follows:

1) Fixing the aluminum block on the upper fixture;
2) Moving the beam down until the positioning semi-circle press a pattern on the aluminum block;
3) Moving the beam up to the original position, control the upper and lower cameras acquire the images of the positioning semi-circle and the pattern respectively;
4) Processing images to get the center coordinates, and calibrating the coefficients a and b by substituting these two coordinates into Equation (1).

The images are shown in Figure 9. The two coordinate points are (878.94, 626.66) and (866.71, 688.95) respectively, and the two coefficients are a=89.1μm and b=-538.1μm.

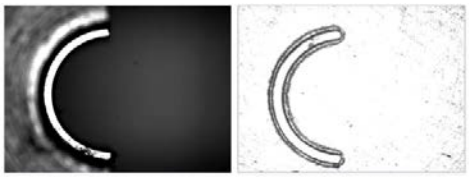

(a) The image of the positioning semi-circle (b) The pattern on the aluminum block

Figure 9. The calibration images of the conversion equation's coefficient

3.2. Measure the Tilt Angle of Guide Rail Z

The procedure to measure the tilt angle (θ_{u1}, θ_{u2}) in U_1V_1W is illustrated as below:

1) Moving the beam up to the original position, open the upper camera and move the camera to the image acquisition position to acquire the image of part A, and save this image;
2) Moving the beam and camera down 10mm, and save the image. Repeat this procedure to get a group of images;
3) Deal with the above images in the image processing software to get the coordinates of the circles' centre. Combine these coordinates with the displacement of the part A along W direction, the movement track of the centre point of part A can be obtained;
4) Fitting space linear equation with the above three-dimensional coordinate points, then the angle (θ_{u1}, θ_{u2}) can be calculated.

By means of the above method, a group of coordinates in $U_1V_1W_1$ was acquired and is shown in Table 2:

Table 2. The path of the camera in U_1V_1W coordinate system

Axis	1/μm	2/μm	3/μm	4/μm	5/μm	6/μm	7/μm
U_1	4108.2	4086.6	4061.1	4059.5	4048.9	4039.1	4028.7
V_1	3265.6	3233.7	3201.3	3189.2	3186.2	3180.8	3182.1
W	0	10000	20000	30000	40000	50000	60000

The coordinates in $U_2V_2W_2$ can be derived based on the Equation (1), and the results are shown in Table 3:

Table 3. The path of the camera in U_2V_2W coordinate system

Axis	1/μm	2/μm	3/μm	4/μm	5/μm	6/μm	7/μm
U_2	4192.5	4171.0	4145.5	4144.0	4133.3	4123.6	4113.2
V_2	2989.2	3021.1	3053.6	3065.6	3068.6	3074.1	3072.9
W	0	10000	20000	30000	40000	50000	60000

The θ_{u1}, θ_{u2}, θ_{l1} and θ_{l2} can be calculated by fitting the space linear equation with the above values. The results are $\theta_{u1} = 0.075°$, $\theta_{u2} = 0.096°$; $\theta_{l1} = 0.075°$, $\theta_{l2} = -0.095°$.

The tilt angle of guide rail X and Y in $U_2O_2V_2$ can use the method which was introduced in Figure 7. In the alignment process, since the two parts can't go beyond the cameras' view, the cameras don't need to move along guide rail X and Y. So the tilt of guide rail X and Y cannot bring the alignment error in. That can be expressed as Equation 10:

$$\begin{bmatrix} \Delta X_u \\ \Delta X_v \end{bmatrix} + \begin{bmatrix} \Delta Y_u \\ \Delta Y_v \end{bmatrix} = \begin{bmatrix} 0 \\ 0 \end{bmatrix}. \tag{10}$$

3.3. Alignment Experiment

In order to verify the feasibility of the error analysis, the imprint method was used again. Firstly, these two cameras were controlled to acquire the images of positioning semi-circle and its pattern after pressing. Then, the upper camera was controlled to move to 40000μm and 60000μm respectively along the guide rail Z. Meanwhile, control the upper camera to acquire the images at these two positions. The images were shown in Figure 10. Processing the images to get the center coordinates. Then, the process results of the upper camera's images were substituted into the transfer equations (Equation (1) and Equation (10)). The results are shown in the Table 4. Finally, the alignment error were calculated. As is shown in Table 5.

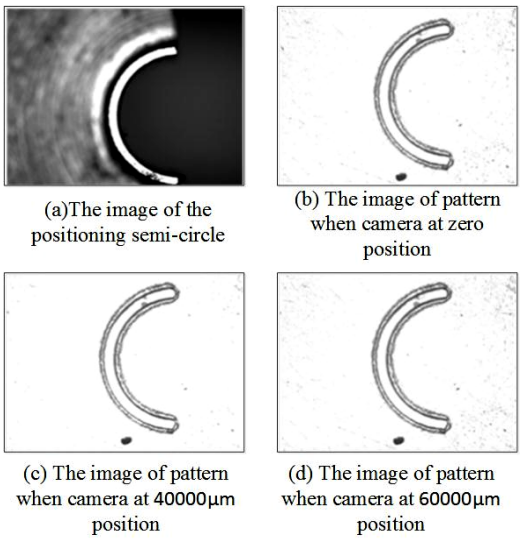

(a)The image of the positioning semi-circle (b) The image of pattern when camera at zero position

(c) The image of pattern when camera at 40000μm position (d) The image of pattern when camera at 60000μm position

Figure 10. Images after alignment

Table 4. The results of the image processing and vision alignment conversion

Positioning semicircle / pixel	ΔL_{z1}/μm	ΔL_{z2}/μm	Pattern/pixel	Before correction/pixel	After correction/pixel
(1162.06, 728.64)	0	0	(1151.84, 587.84)	(1162.45, 726.64)	(1162.45, 726.64)
	40000	0	(1141.09, 569.49)	(1151.80, 744.89)	(1162.70, 730.63)
	60000	0	(1136.28, 564.63)	(1147.03, 749.73)	(1163.38, 728.34)

Table 5. The alignment error of the instrument

ΔL_{z1}/μm	Alignment error/μm	
	Before correction	After correction
0	(1.86, -7.68)	(1.86, -7.68)
40000	(-48.94, 77.51)	(3.05, 9.49)
60000	(-62.20, -100.60)	(6.30, -1.43)

As shown in Table 5, the alignment error caused by the tilt of guide rail is large, and it will directly lead to the failure of assembly work. But, the alignment error is greatly reduced after adding compensation, the alignment accuracy affected by ΔL_{z1} is not obvious, and the alignment accuracy of the press-fit instrument can achieve the requirement of assembly work.

4. Conclusion

In this paper, based on the developed precision press-fit instrument, the visual alignment device which is composed of camera and three-dimensional precision displacement platform was introduced. For this kind of VAD, the alignment error caused by the tilt of camera guide rail Z had been analyzed, and the error influence equation was derived. Combined with the analysis results, the final transfer equation between two cameras was given. Experimental results demonstrated that final transfer equation can help the press-fit instrument improve the alignment accuracy effectively. The alignment accuracy can reach ±10μm, and the instrument becomes more flexible, and it can accomplish the assembly work of the small interference fitting parts with different sizes.

Acknowledgements

The authors gratefully acknowledge the Financial Support by the National Science and Technology Major Project (Project no. 2013ZX04001091), the National Science-technology Support Plan Project (Project no. 2014BAF08B02), and the Fundamental Research Fund for the Central Universities (Project no. DUT16RC(3)034).

References

[1] Wang X D, Hongxia Song, Chao Liu, et al. Automatic measurement and assembly of miniature partsbased on machine vision. Journal of Harbin Engineering University, 2011, 32(9): 1117-1122.

[2] Wu J D, Bin H Z. Dimensional inspecting system of thin sheet parts based on machine vision. Optics and Precision Engineering, 2007, 15(1): 124-130.

[3] Wang L Q, Liu Z, Zhang Z H. Accurate dimensional measurement of special circle arcs based on stereo vision. Chinese journal of scientific instrument, 2013, 34(10): 2395-2400.

[4] Qiao Y J, Wang H R, Zhao Y J. Study on binocular vision measurement network layout for large curved surface parts. Chinese journal of scientific instrument, 2015, 36(4): 913-918.

[5] Xiao Y Y, Zhang J H. The Automatic Alignment System for Laser Bonding Based on Visual Identification and Location. Intelligent Robotics and Applications, 2015, 9245: 533-541.

[6] Ye X, Gao J, Zhang Z J, et al. An improved vision calibration method for coaxial alignment microassembly. Assembly Automation, 2014, 34(3):237-243.

[7] Liu G H, Wang W B, Yuan J Y, et al. A Novel Camera Calibration Method of Variable Focal Length Based on Single-View. 2009 Second International Symposium on Electronic Commerce and Security, Nanchang, China, 2009:125-128.

[8] Pu Z B, Qu Y F, Wang Y A. Study of Illumination in Vision Measuring System. Chinese journal of scientific instrument, 2003, 24(4): 438-439.

[9] Tang Y L, Zhang Z J, Ye X, et al. Micro-assembly precise coaxial alignment methodology based on surface roughness and reflectiveness matching. *Assembly Automation*, 2014, 34(2): 141-151.

[10] Daljae Lee, Xiaodong Tao, Hyungsuck Cho, et. Flip-chip alignment with a dual imaging system using a visual servoing method. Optomechatronic Systems Control, 2005, 6052, 605203.

[11] Y. S. Ihn et al. "An Enhanced Vision Processing Algorithm for a Micro-manipulation System," 2007 International Workshop on Robotic and Sensors Environments, Ottawa, Ont, 2007, pp. 1-6.

[12] Nian C Y, Tang Y S. An auto-alignment vision system with three-axis motion control mechanism. Int J Adv Manuf Technol, 2005, 26: 1121-1131.

[13] Tang Q J, Tian X F, Geng M C, et. Global calibration method for CCD based visual inspective system. Optics and Precision Engineering, 2011, 19(8): 1903-1910.

[14] Lou Z F, Wang X D, You B, et al. Pressing-fitting technology and instrument for precision small parts. Optics and Precision Engineering, 2015, 23(6): 1605-1011.

[15] Yang Xu. Control and System Calibration of the Precision Press-fit Assembly Device for Miniature Components.